Urinary metabolomics in *Fxr*-null mice reveals activated adaptive metabolic pathways upon bile acid challenge

Joo-Youn Cho,* Tsutomu Matsubara,* Dong Wook Kang,† Sung-Hoon Ahn,* Kristopher W. Krausz,* Jeffrey R. Idle,§ Hans Luecke,† and Frank J. Gonzalez[1,*]

Laboratory of Metabolism,* Center for Cancer Research, National Cancer Institute, and Laboratory of Bioorganic Chemistry,† National Institute of Diabetes and Digestive and Kidney Diseases, National Institutes of Health, Bethesda, MD; and Institute of Pharmacology,§ Charles University, First Faculty of Medicine, Prague, Czech Republic

Abstract **Farnesoid X receptor (FXR) is a nuclear receptor that regulates genes involved in synthesis, metabolism, and transport of bile acids and thus plays a major role in maintaining bile acid homeostasis. In this study, metabolomic responses were investigated in urine of wild-type and *Fxr*-null mice fed cholic acid, an FXR ligand, using ultra-performance liquid chromatography (UPLC) coupled with electrospray time-of-flight mass spectrometry (TOFMS). Multivariate data analysis between wild-type and *Fxr*-null mice on a cholic acid diet revealed that the most increased ions were metabolites of *p*-cresol (4-methylphenol), corticosterone, and cholic acid in *Fxr*-null mice. The structural identities of the above metabolites were confirmed by chemical synthesis and by comparing retention time (RT) and/or tandem mass fragmentation patterns of the urinary metabolites with the authentic standards. Tauro-3α,6,7α,12α-tetrol (3α,6,7α,12α-tetrahydroxy-5β-cholestan-26-oyltaurine), one of the most increased metabolites in *Fxr*-null mice on a CA diet, is a marker for efficient hydroxylation of toxic bile acids possibly through induction of *Cyp3a11*. A cholestatic model induced by lithocholic acid revealed that enhanced expression of *Cyp3a11* is the major defense mechanism to detoxify cholestatic bile acids in *Fxr*-null mice. These results will be useful for identification of biomarkers for cholestasis and for determination of adaptive molecular mechanisms in cholestasis.**—Cho, J. Y., T. Matsubara, D. W. Kang, S. H. Ahn, K. W. Krausz, J. R. Idle, H. Luecke, and F. J. Gonzalez. **Urinary metabolomics in *Fxr*-null mice reveals activated adaptive metabolic pathways upon bile acid challenge. *J. Lipid Res.* 2010.** 51: **1063–1074.**

Supplementary key words adaptive response • cholic acid • corticosterone • *Cyp3a11* • farnesoid X receptor • lithocholic acid • metabolomics • *p*-cresol

The farnesoid X receptor (FXR; NR1H4) is a nuclear receptor that is activated by a number of bile acids including cholic acid, chenodeoxycholic acid, and lithocholic acid. Activated FXR forms a heterodimer with retinoid X receptors (RXR; NR1B) and binds its response elements usually located upstream of FXR target genes (1, 2). FXR regulates genes involved in synthesis, metabolism, and transport of bile acids in liver and gut, thereby maintaining bile acid homeostasis. Bile acids are produced from cholesterol in liver by bile acid synthetic enzymes, such as CYP7A1 and CYP8B1 (3), and are excreted into bile through canalicular bile acid transporters, such as bile salt export pump (BSEP) and MRP2 (4). However, under the condition of excessive bile acid loading such as in experimental cholestasis in mice, FXR is strongly activated by bile acids, downregulates the expression of *Cyp7a1* and *Cyp8b1*, upregulates bile acid transporters, following which serum and liver bile acid levels are decreased (5).

The critical role of FXR in bile acid homeostasis was established using mice with targeted disruption of *Fxr* (*Fxr*-null mice) (6). *Fxr*-null mice, under conditions of bile acid loading such as cholic acid feeding and common bile duct ligation, had increased serum and liver bile acid levels and decreased fecal bile acid excretion because of reduced expression of the bile acid export pump BSEP (6). In addition, excretion of urinary bile acids was increased in *Fxr*-null mice fed diets containing 1% cholic acid, suggest-

This work was supported by the National Cancer Institute Intramural Research Program. Its contents are solely the responsibility of the authors and do not necessarily represent the official views of the National Institutes of Health. This work was also supported by Grant A03001 (J.Y.C.) from the Korea Health 21 R&D Project, Ministry of Health and Welfare, Republic of Korea and by a grant for collaborative research (J.R.I.) from the United States Smokeless Tobacco Company.

Manuscript received 5 October 2009 and in revised form 9 November 2009.

Published, JLR Papers in Press, November 9, 2009
DOI 10.1194/jlr.M002923

Abbreviations: ALP, alkaline phosphatase; ALT, alanine aminotransferase; CA, cholic acid; CAR, constitutive androstane receptor; CYP, cytochrome P450; DHOPA, 11β,20-dihydroxy-3-oxopregn-4-en-21-oic acid; FXR, farnesoid X receptor; HDOPA, 11β-hydroxy-3,20-dioxopregn-4-en-21-oic acid; LCA, lithocholic acid; MS/MS, tandem mass spectrometry; OPLS, orthogonal partial least squares; PCA, principal components analysis; PLS-DA, partial least-squares discriminant analysis; PPARα, peroxisome proliferator-activated receptor α; PXR, pregnane X receptor; qPCR, quantitative real-time polymerase chain reaction; RT, retention time; TOFMS, time-of-flight mass spectrometry; UPLC, ultra-performance liquid chromatography.

[1]To whom correspondence should be addressed.
e-mail: fjgonz@helix.nih.gov

ing that the metabolic pathways of controlling bile acid levels might be altered in *Fxr*-null mice (6). Recently, an adaptive response to bile acids in *Fxr*-null mice was reported. Loss of FXR leads to increased susceptibility to bile acid-induced liver injury and results in adaptive changes of genes involved in regulation of basolateral bile acid uptake, bile acid metabolism/detoxification, and alternative basolateral bile acid secretion in an FXR-independent manner (7, 8).

Metabolomics, the global approach for identification and quantification of metabolites in a living system or biological sample has been mostly performed using nuclear magnetic resonance (NMR) spectroscopy or mass spectrometry (MS) combined with various multivariate data analyses (9). Recently, robust metabolomic methods using the high resolution capability of ultra-performance liquid chromatography (UPLC) coupled with the accurate mass determination of time-of-flight (TOF) MS were developed for detection and characterization of small organic molecules in complex biological matrices (10). A recent metabolomics study, combined with a genetically modified knockout mouse, has revealed that activation of peroxisome proliferator-activated receptor α (PPARα) affects the metabolism of tryptophan, corticosterone, and fatty acids, and that novel steroid metabolites, 11β-hydroxy-3,20-dioxopregn-4-en-21-oic acid (HDOPA) and 11β,20-dihydroxy-3-oxopregn-4-en-21-oic acid (DHOPA), in urine can be biomarkers for activation of PPARα (11). More recently, a metabolomics study on the activation of pregnane X receptor (PXR) was performed using urine from *Pxr*-null mice and their congenic wild-type counterparts treated with the PXR ligand, pregnenolone 16α-carbonitrile (12). A novel vitamin E metabolite, γ-CEHC glucoside, and α-CEHC glucuronide were strongly decreased upon activation of PXR and might serve as biomarkers for PXR activation. Thus, metabolomics revealed PXR-activated metabolic pathways associated with vitamin E metabolism (12). These studies highlight that metabolomics can be useful to identify small molecule signatures for gene deficiency and activation of nuclear receptors and/or their pathophysiological stimuli.

In the present study, altered metabolomic responses were investigated in urine of *Fxr*-null mice administered cholic acid compared with wild-type mice. UPLC-TOFMS coupled with multivariate data analyses were used to distinguish between the urinary metabolites in *Fxr*-null and wild-type mice on the CA diet. The structure of novel metabolites was identified and those metabolites were quantified using synthetic standards. This study further revealed adaptive molecular mechanisms for activation of alternate metabolic pathways in the cholestatic *Fxr*-null mouse.

EXPERIMENTAL PROCEDURES

Reagents

Standards for taurocholate, tauro-β-muricholate and reagents for synthesis were purchased from Sigma (St. Louis, MO). HDOPA and DHOPA were purchased from Anbilaunch consulting (San Meteo, CA). HPLC-grade solvents (acetonitrile, methanol, and water) were purchased from Fisher Scientific (Hampton, NH).

Animals, diets, and sample collection

Fxr-null mice and the background matched wild-type mice generated as reported previously (6) were maintained under a standard 12-h light/12-h dark cycle with water and a normal diet (NIH-31) provided ad libitum. Groups of 8- to 12-week-old male mice were put on a synthetic purified diet (AIN-93G, Bio-Serv) at day 5 before treatment and maintained with water and the same diet ad libitum. The CA diet and LCA diet consisted of the control diet (AIN-93G) supplemented with 1% (w/w) CA and 0.6% (w/w) lithocholic acid, respectively. *Fxr*-null and wild-type mice were fed the CA diet or control diet for 7 days and the LCA diet or control diet for 4 days. Urine samples were collected from mice placed individually in metabolic cages for 24 h, before treatment and on day 6 of CA treatment or day 3 of LCA treatment. All urine samples were stored at –80°C until analyzed. At the end of the study, animals were killed, and serum and liver tissue were collected and frozen at –80°C for further analysis. Protocols for all animal studies were approved by the National Cancer Institute Animal Care and Use Committee and were carried out in accordance with the guidelines of Institute of Laboratory Animal Resources.

Serum chemistry

Serum was prepared by centrifugation at 8,000 rpm for 10 min and the catalytic activities of alanine aminotransferase (ALT) and alkaline phosphatase (ALP) were measured in serum. Briefly, 2 μl of serum was mixed with 200 μl of ALT or ALP assay buffer (Catachem, Bridgeport, CT) in a 96-well microplate and monitored at 340 nm or 405 nm for 10 min at 37°C. Serum corticosterone levels were determined using a Corticosterone EIA Kit (Cayman Chemical Co., Ann Arbor, MI) according to the manufacturer's instruction.

UPLC-TOFMS analyses

Urine aliquots were diluted with 4 vols of 50% acetonitrile and centrifuged at 18,000 *g* for 20 min at 4°C to remove particles and proteins. The aliquots (5 μl) were injected into a reverse-phase 50 × 2.1 mm ACQUITY® 1.7-μm BEHC18 column (Waters Corp., Milford, MA) using an ACQUITY® UPLC system (Waters) with a gradient mobile phase comprising 0.1% formic acid (A) and acetonitrile containing 0.1% formic acid (B). Each sample was resolved for 10 min at a flow rate of 0.5 ml/min with the gradient consisted of 100% A for 0.5 min, 20% B for 3.5 min, 95% B for 4 min, 100% B for 1 min, and 100% A for 1 min. The eluent was introduced by electrospray ionization into the mass spectrometer, Q-TOF Premier® (Waters), operating in either negative ion (ESI−) or positive ion (ESI+) electrospray ionization modes. The capillary and sampling cone voltages were set to 3000 and 30 V, respectively. The desolvation gas flow was set to 650 L/h and the temperature was set to 350°C. The cone gas flow was 50 L/h, and the source temperature was 120°C. To maintain mass accuracy, sulfadimethoxine ($[M-H]^-$ 309.0658) at a concentration of 250 pg/μl in 50% acetonitrile was used as a lock mass and injected at a rate of 30 μl/min. Data were acquired in centroid mode from 50 to 800 *m/z* in MS scanning. Tandem MS collision energy was scanned from 5 to 35 V.

Data processing and multivariate data analysis

Centroided and integrated chromatographic mass data from 50 to 800 *m/z* were processed by MarkerLynx® (Waters) to generate a multivariate data matrix. Pareto-scaled MarkerLynx matri-

ces including information on sample identity were analyzed by principal components analysis (PCA) and partial least-squares discriminant analysis (PLS-DA) using SIMCA-P+ 12 (Umetrics, Kinnelon, NJ). To determine which ions contribute to the difference between wild-type (y = 0) and *Fxr*-null (y = 1) mice of the CA-fed group, orthogonal partial least squares (OPLS) was used. The loadings scatter S-plots and the contribution lists were used to describe the candidate markers that were significantly different between wild-type and *Fxr*-null mice of CA-fed group.

Identification of metabolites

To identify the structure of high-contribution score metabolites, elemental compositions were generated with MassLynx® (Waters) based on the exact masses of the top twelve ions. To confirm the identities of markers, authentic standards at 5–20 μM in 50% acetonitrile were compared with the urine sample on the condition of MS/MS fragmentation with collision energy ramping from 15 to 35 V. Therefore, the MS/MS fragmentation spectrum of putative urine metabolites was shown to be identical to that of the authentic standards.

Synthesis of *p*-cresol sulfate and glucuronide

p-Cresol sulfate was prepared by treating *p*-cresol with chlorosulfonic acid in methylene chloride. To synthesize *p*-cresol glucuronide, *p*-cresol was reacted with tetraacetylglucuronyl trichloroimidate in the presence of boron trifluoride diethyl etherate in methylene chloride to afford *p*-cresol tetraacetyl glucuronide (13). The product was hydrolyzed with 2M potassium hydroxide in methanol to obtain *p*-cresol glucuronide.

Synthesis of bile acid metabolites

Synthesis of (3α,6α/β,7α/β,12α)-tetrahydroxy-5β-cholanic acids (4 epimers) have been reported (14). Synthesis of 3α,7β,12α-trihydroxy-5β-cholanic acid also followed this method. All stereoisomeric bile acids were synthesized from cholic acid. Taurine conjugates of 5β-cholanic acids were synthesized by two-step reactions (15, 16). The first step was to prepare pentafluorophenyl esters where 5β-cholanic acids reacted with pentafluorophenol in the presence of 1-(3-dimethylaminopropyl)-3-ethylcarbodiimide hydrochloride and a catalytic amount of *N*,*N*-dimethylformamide in methylene chloride. The second step was the reaction of 5β-cholanic acid pentafluorophenyl esters and taurine in 1,8-diazabicyclo[5,4,0]undec-7-ene as a base in methylene chloride to synthesize taurine conjugates of bile acids. Although most of 5β-cholanic acid taurine conjugates are very polar compounds, they can be purified by a general silica gel column chromatography method eluting with gradient of 5-25% methanol in methylene chloride. To isolate taurine conjugates by this general column chromatography method, 1% acetic acid was added to the eluting solvent. All 5β-cholanic acids and their taurine conjugates have good solubility in water and methanol.

Quantification of urinary metabolites

QuanLynx® (Waters) was used to quantify urinary creatinine, HDOPA, DHOPA, taurocholate, tauro-7-epicholate, and tauro-3,6,7,12-tetrol from their peak areas. One μM of dehydrocholate ($[M-H]^-$ 401.2330) was included as an internal standard. Calibration curves were constructed from 50 to 1000 μM of creatinine ($[M+H]^+$ 114.0670) and from 1 to 100 μM of HDOPA ($[M-H]^-$ 359.1843), DHOPA ($[M-H]^-$ 361.2008), taurocholate ($[M-H]^-$ 514.2831 and RT 5.5 min), tauro-7-epicholate ($[M-H]^-$ 514.2822 and RT 5.0 min) and tauro-3,6,7,12-tetrol ($[M-H]^-$ 530.2779). The concentration of each analyte in mouse urine was determined from the calibration curves using linear regression analysis. All determined correlation coefficients were >0.95 for each analyte, and the resultant concentrations were expressed as μmol/mmol creatinine (normalized).

Gene expression analysis

Quantitative real-time PCR (qPCR) was performed using cDNA generated from 1 μg total mRNA SuperScript II Reverse Transcriptase kit (Invitrogen, Carlsbad, CA). Primers were designed for qPCR using the Primer Express software (Applied Biosystems, Foster City, CA) based on GenBank sequence data: *Cyp3a11*: forward 5′-ttctgtcttcacaaaccggc-3′; reverse 5′-gggggacagcaaagctctat-3′, *Cyp2b10*: forward 5′-tcttgcgcctgctgcag-3′; reverse 5′-tggctggagaatgagcttatgag-3′ and *Actb*: forward 5′-ttctttgcagctcctcgtt-3′, reverse 5′-atggaggggaatacagccc-3′. qPCR reactions were performed with the cDNA, the primer sets and SYBR Green PCR Master Mix (Applied Biosystems, Foster City, CA) and demonstrated by an Applied Biosystems Prism 7900HT Sequence Detection System. Relative mRNA levels were calculated by the comparative threshold cycle method using β-actin (*Actb*) as the internal control.

Statistical analysis

Each group consisted of 6–12 animals for this study. All values are expressed as the means ± SD. Statistical analysis was performed by two-way ANOVA combined with Bonferroni posttests using Prism 5 (GraphPad Software Inc., San Diego, CA). Correlations between relative *Cyp3a11* levels and relative abundance of taurotetrol or ALT activity were calculated using Pearson correlation tests (Prism 5). A *P* value of less than 0.05 was considered statistically significant.

RESULTS

Phenotypes of *Fxr*-null mice

Male wild-type and *Fxr*-null mice fed a control diet showed no significant differences in body weight, liver-to-body weight ratio, and serum ALP activity (**Table 1**). However, after feeding 1% CA for 7 days, *Fxr*-null mice exhibited more severe body weight loss, higher liver-to-body weight ratios, and higher serum ALP activity than wild-type mice (Table 1). These phenotypes are similar with those previously reported for wild-type and *Fxr*-null mice after feeding CA (17). In contrast, the typical diagnostic hepatotoxicity marker, serum ALT activity, was two-fold higher in *Fxr*-null mice than in wild-type mice fed control diet but was not significantly changed between *Fxr*-null and wild-type mice

TABLE 1. Changes in body weight, liver- to body weight ratio, and liver toxicity

Diagnostic Marker	Control		CA-Fed	
	Wild-Type Mice	*Fxr*-Null mice	Wild-Type Mice	*Fxr*-Null Mice
BW (%)	101.5 ± 2.7	102.7 ± 1.6	90.7 ± 8.9	73.3 ± 4.16[b]
LW/BW ratio	3.92 ± 0.21	3.79 ± 0.12	3.61 ± 0.45	5.08 ± 0.46[b]
ALT (IU/l)	71.7 ± 20.1	141.4 ± 62.8[a]	1240 ± 1110	1810 ± 625
ALP (IU/l)	163 ± 18.2	221 ± 102	165 ± 58.0	456 ± 91.0[b]

Comparison of diagnostic markers between wild-type and Fxr-null mice in either control or cholic acid-treated groups (n = 4–12). Values are means ± SD. ALP, alkaline phosphatase; ALT, alanine aminotransferase; BW, body weight; FXR, farnesoid X receptor; LW, liver weight.

[a] $P < 0.01$ compared with wild-type mice.

[b] $P < 0.001$ compared with wild-type mice.

fed CA, which suggested that *Fxr*-null mice under bile acid-loading conditions exhibited FXR-dependent cholestasis, but showed similar sensitivity to bile acid-induced hepatotoxicity compared with CA fed wild-type mice.

Metabolomic analysis of mouse urine

Urine samples for 0–24 h were collected before and after six days of CA feeding and analyzed by UPLC-TOFMS operating in both positive and negative ionization modes. Bile acids showed several fragment ions derived from only one bile acid in positive ion mode and thus multivariate data analysis was performed on the data matrix from the negative ionization mode. A large data matrix containing approximately 6000 ions was produced by MarkerLynx and subjected to both PCA and PLS-DA multivariate data analyses. Unsupervised PCA yielded a good separation of the data sets from the control and CA-fed groups in both wild-type and *Fxr*-null mice, with fitness (R^2 value) of 0.52 and prediction power (Q^2 value) of 0.28 (data not shown). A supervised PLS-DA model with six components successfully discriminated the differences between all four groups of mice, having cumulative fitness (R^2X and R^2Y values) of 0.65 and 0.96, respectively, and cumulative prediction power (Q^2 value) of 0.80. **Fig. 1A** shows a PLS-DA scores plot providing a clear separation between wild-type ($^{+/+}$) and *Fxr*-null ($^{-/-}$) mice of CA-fed groups in component 1 (Y-axis) but not in the control diet group. This result revealed that more specific metabolic phenotypes were changed in *Fxr*-null mice than in wild-type mice by CA loading. After OPLS analysis of wild-type and *Fxr*-null mice in the CA-fed groups, a loadings S-plot showed ions with the highest confidence and greatest contribution to separation between wild-type and *Fxr*-null mice in the CA-fed groups (Fig. 1B). The significant ions increased in *Fxr*-null mice after CA loading were in the upper-right quadrant and those decreased were in the lower-left quadrant. The increased negative ions were labeled with a number from 1 to 12 according to the highest confidence and greatest contribution to separation between wild-type and *Fxr*-null mice in CA-fed groups in Fig. 1B. Three types of metabolites, specifically *p*-cresol, corticosterone, and cholic acid metabolites, were confirmed from the data (**Table 2**). To identify the structure of the above ions, accurate mass values of each ion was used for chemical formula calculations using elemental composition and mass-based searches in various database/literature were performed. Both 187.0060 (1; $[M-H]^-$) and 397.0009 (9; $[2M-2H+Na]^-$) ions correspond to *p*-cresol sulfate, and the 283.0812 (3; $[M-H]^-$)

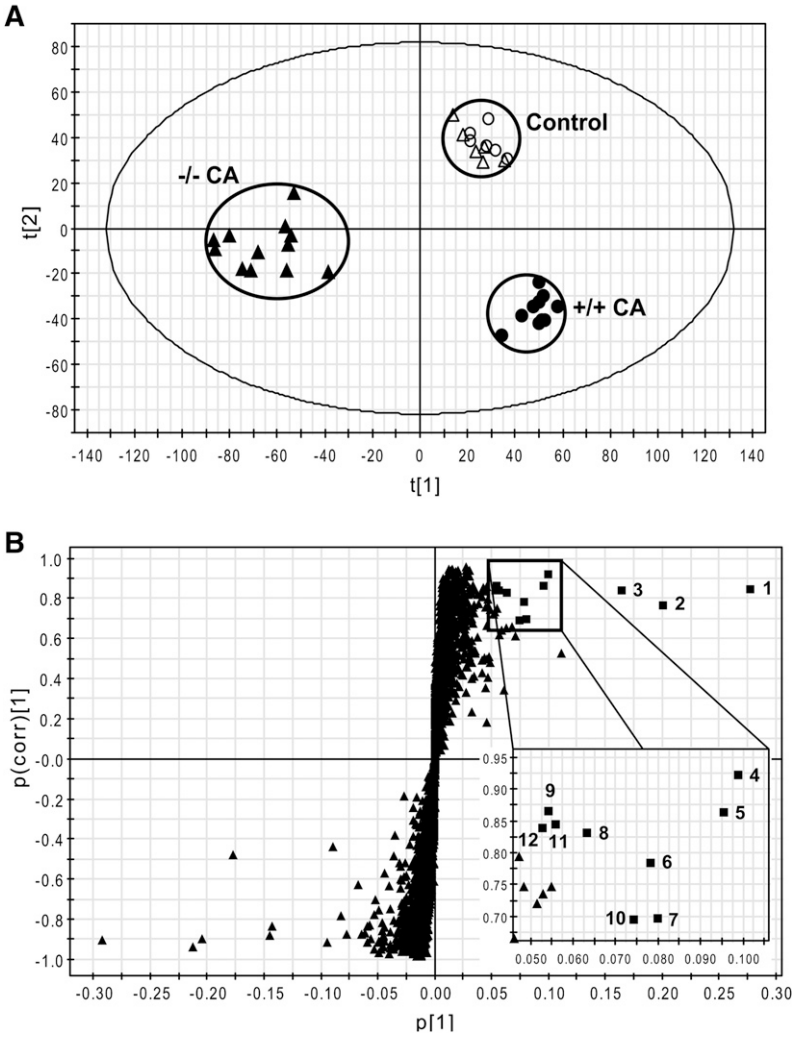

Fig. 1. Metabolomic analysis of control diet- and CA diet-fed mouse urine. Wild-type and *Fxr*-null mice (n = 6–12) were fed with control diet or 1% CA containing diet for 7 days. Urinary metabolites were analyzed by UPLC-TOFMS and data processing and multivariate data analysis conducted using MarkerLynx and SIMCA-P+ software, respectively. A: Scores scatter plot of PLS-DA model of urine from the control and CA-treated groups in both wild-type ($^{+/+}$) and *Fxr*-null ($^{-/-}$) mice. A six-component PLS-DA model was constructed to characterize the relationship among four mouse groups, including wild-type (control, open circle; CA-fed, closed circle) and *Fxr*-null (control, open triangle; CA, closed triangle). The t(1) and t(2) values represent the scores of each sample in principal components 1 and 2, respectively. The cumulative fitness (R^2X and R^2Y values) and prediction power (Q^2 value) of this six-component model are 0.65, 0.96, and 0.80, respectively. B: OPLS loadings S-plot comparing *Fxr*-null mice versus wild-type mice in CA-fed groups. The *x* axis is a measure of the relative abundance of the ions, and the *y* axis is a measure of the correlation of each ion to the model. Negative ions located in the upper right quadrant are increased when comparing *Fxr*-null mice with wild-type mice in CA-fed groups. Labeling of significant ions increased (closed square) is the same as in Table 1. CA, cholic acid; FXR, farnesoid X receptor; TOFMS, time-of-flight mass spectrometry; UPLC, ultra-performance liquid chromatography.

TABLE 2. Summary of negative metabolite ions showing significant increase in urine concentration of CA-fed *Fxr*-null mice

Ion Rank	RT (min)	Mass (*m/z*)	Identity	Empirical Formula	Mass Error (ppm)	Fold Change (*Fxr*-null/WT)
p-Cresol metabolites						
1	3.41	187.006	*p*-Cresol sulfate	C7H8O4S	2.5	5
3	3.53	283.0812	*p*-Cresol glucuronide	C13H16O7	2.0	8
9	3.40	397.0009	*p*-Cresol sulfate_dimer+Na	C14H16O8S2Na	4.6	9
Corticosterone metabolites						
4	5.29	361.2008	DHOPA	C21H30O5	1.9	18
5	5.39	359.1843	HDOPA	C21H28O5	4.4	50<
6	4.66	377.1943	Hydroxylated DHOPA[a]	C21H30O6	5.5	50<
10	4.54	375.1799	Hydroxylated HDOPA[a]	C21H28O6	2.3	50<
Cholic acid metabolites						
2	4.79	530.2779	Tauro-3α,6,7α,12α-tetrol	C26H45NO8S	1.6	50<
7	5.50	514.2831	Taurocholate	C26H45NO7S	1.5	5
8	5.37	569.3306	Cholate glucoside[a]	C30H50O10	3.5	12
11	5.00	514.2822	Tauro-7-epicholate	C26H45NO7S	3.2	50<
12	5.15	676.3354	Taurocholate glucoside[a]	C32H55NO12S	1.9	50<

CA-fed *Fxr*-null mice compared with CA-fed wild-type mice (n = 12). Conditions for UPLC-TOFMS analysis are described in "Experimental Procedures." Ion rank from a loading S-plot of OPLS analysis showed the rank of ions with the highest confidence and greatest contribution to separation between wild-type and *Fxr*-null mice. Ion rank is the same as labeling of ions in Fig. 1B. Fold change equals the fold increase in the level observed in *Fxr*-null mice group compared with wild-type mice group. CA, cholic acid; FXR, farnesoid X receptor; RT, retention time; TOFMS, time-of-flight mass spectrometry; UPLC, ultra-performance liquid chromatography; WT, wild type.

[a] Structural identities of these metabolites were not elucidated.

ion corresponds to *p*-cresol glucuronide. Generation of the isomeric *o*-cresol and *m*-cresol sulfates in situ by the sulfation of *o*- and *m*-cresol with fuming sulfuric acid revealed that the three isomeric sulfates could not be resolved by UPLC and that they had virtually identical MS/MS spectra (data not shown). Accordingly, urines were hydrolyzed with 5M HCl at 100°C, neutralized, subjected to solid phase extraction, eluted and then, together with authentic *o*-, *m*-, and *p*-cresol, derivatized with BSTFA to yield the trimethylsilyl derivatives of the cresol isomers. GCMS analysis revealed that the cresol present in urine as its sulfate and glucuronide was almost exclusively *p*-cresol (data not shown). The 361.2008 (4; $[M-H]^-$) and 359.1843 (5; $[M-H]^-$) ions correspond to DHOPA and HDOPA, respectively, according to a previous report (11). The 377.1943 (6; $[M-H]^-$) and 375.1799 (10; $[M-H]^-$) ions are novel ions that are proposed to be hydroxylated DHOPA and HDOPA, respectively. The 530.2779 (2; $[M-H]^-$), 514.2831 (**7**; $[M-H]^-$), 569.3306 (8; $[M-H]^-$), 514.2822 (11; $[M-H]^-$) and 676.3354 (12; $[M-H]^-$) ions correspond to tauro-3α,6,7α,12α-tetrol, taurocholate, cholate glucoside, tauro-7-epicholate, and taurocholate glucoside, respectively. Because the basal levels of the metabolite ions, 2, 5, 6, 10, 11, and 12 were very low, the values of fold change in each metabolite were over 50. However, the chemical structures still required experimental verification using the authentic compounds.

Identification and quantification of *p*-cresol metabolites

Authentic *p*-cresol sulfate and *p*-cresol glucuronide were required to confirm the structural identification of these metabolites by UPLC-MS/MS and to quantify the levels of these metabolites. The *p*-cresol sulfate and *p*-cresol glucuronide were synthesized and the MS/MS structural elucidation of *p*-cresol sulfate ($[M-H]^-$ = 187.006) in negative ion mode was carried out (**Fig. 2A**). The major daughter ions 107 and 79.9 in negative ion mode were interpreted in the inlaid structural diagram. In addition, the MS/MS structural elucidation of *p*-cresol glucuronide ($[M-H]^-$ = 283.0812) in negative ion mode was performed (Fig. 2B). The major daughter ions 175 and 107 in negative ion mode were interpreted in the inlaid structural diagram. Because of the insufficient purity of synthetic standards, proper calibration curves could not be constructed for both *p*-cresol sulfate and *p*-cresol glucuronide. Therefore, relative abundance of *p*-cresol sulfate and *p*-cresol glucuronide were measured in each urine sample and expressed as response/mmol creatinine, a variable independent of urine volume. Although the relative abundance of *p*-cresol sulfate and *p*-cresol glucuronide were decreased significantly in both wild-type and *Fxr*-null mice after CA feeding ($P < 0.001$), the wild-type mice on the CA diet exhibited a significant and dramatic depletion of urinary *p*-cresol sulfate (8.3% of control, $P < 0.001$, Fig. 2C) and *p*-cresol glucuronide (4.5% of control, $P < 0.001$, Fig. 2D). Therefore, the *Fxr*-null mice on the CA diet exhibited significantly greater than wild-type mice on the CA diet by 4-fold ($P < 0.01$) or 10-fold ($P < 0.001$) in either *p*-cresol sulfate or *p*-cresol glucuronide urine levels, respectively (Fig. 2C, D).

Identification and quantification of glucocorticoid metabolites

To identify the structure of hydroxylated HDOPA and DHOPA, authentic compounds of 19-hydroxylated HDOPA and 19-hydroxylated DHOPA were synthesized and tandem MS fragmentation was performed. The patterns of MS/MS spectra between the synthetic compounds and the hydroxylated metabolites in mouse urine were different (data not shown), suggesting that the hydroxylated HDOPA and DHOPA is not 19-hydroxyl HDOPA and 19-hydroxyl DHOPA. The identities of HDOPA and DHOPA were established by comparison of MS/MS frag-

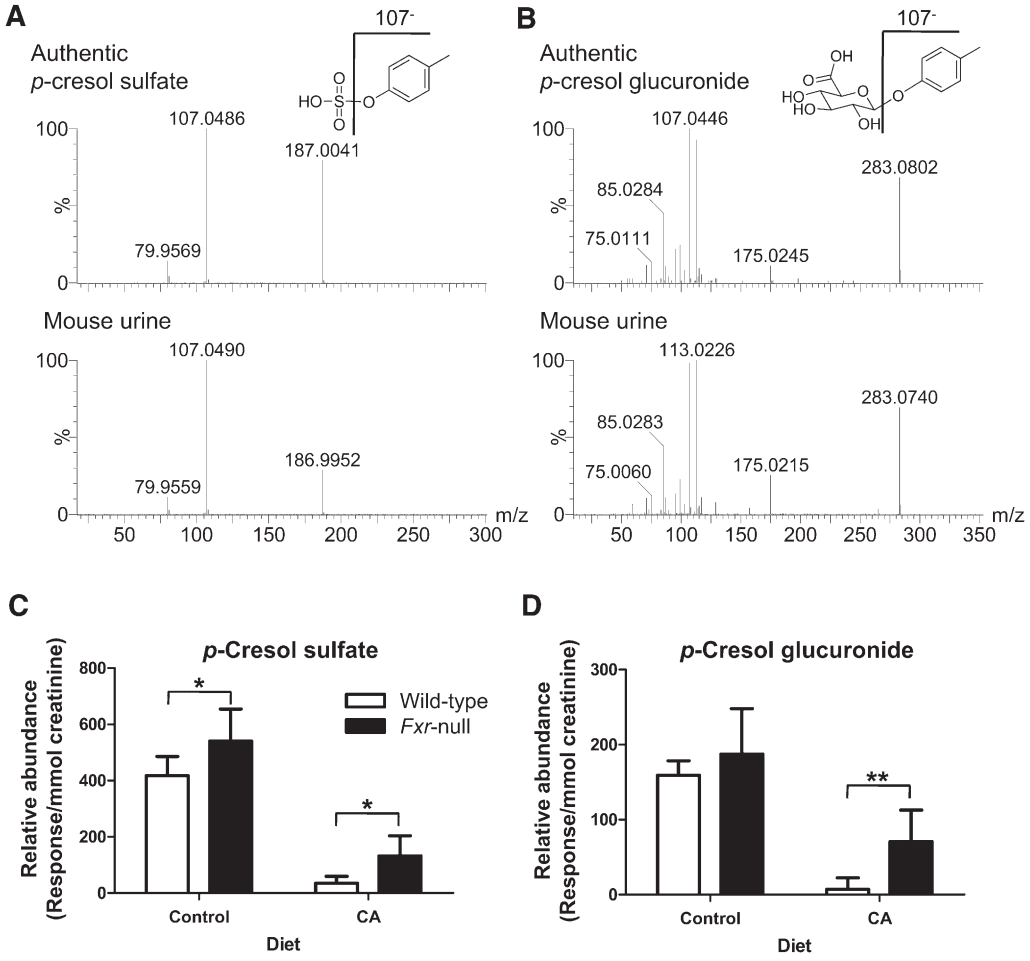

Fig. 2. Identification and characterization of *p*-cresol sulfate and *p*-cresol glucuronide. A: MS/MS spectrum of authentic *p*-cresol sulfate and metabolite 1 from mouse urine in negative ion mode. MS/MS fragmentation was conducted with collision energy ramping from 5 to 35 eV. Major daughter ions from MS/MS fragmentation were interpreted in the inlaid structural diagrams. B: MS/MS spectrum of authentic *p*-cresol glucuronide and metabolite 3 from mouse urine in negative ion mode. MS/MS fragmentation was conducted with same condition as *p*-cresol sulfate. C: Relative abundance of *p*-cresol sulfate in the 24-h urine of wild-type and *Fxr*-null mice treated with 1% CA or control for 7 days. Relative abundance of *p*-cresol sulfate (mean ± SD) was determined by the peak area responses of *p*-cresol sulfate normalized by the creatinine concentration in urine. D: Relative abundance of *p*-cresol glucuronide (mean ± SD) was determined by the peak area responses of *p*-cresol glucuronide normalized by the creatinine concentration in urine. Open and filled bars represent wild-type and *Fxr*-null mice groups, respectively. The *P* values were calculated by ANOVA with Bonferroni posttests. $*P < 0.01$ and $**P < 0.001$ compared with wild-type mice. CA, cholic acid; FXR, farnesoid X receptor; MS/MS, tandem mass spectrometry.

mentation of authentic standards and the urinary compounds as demonstrated in the previous report (11). In addition, the concentrations of HDOPA and DHOPA in urine were determined using calibration curves. Whereas both wild-type and *Fxr*-null mice fed control diet had undetectable HDOPA and DHOPA in their urine, *Fxr*-null mice fed CA diet only had 229 ± 92 μmol/mmol creatinine in HDOPA and 110 ± 25 μmol/mmol creatinine in DHOPA (**Fig. 3A**, B). Moreover, the relative abundance of hydroxylated HDOPA and DHOPA was significantly increased in *Fxr*-null mice fed CA diet as a similar pattern to the concentration of HDOPA and DHOPA (Fig. 3C, D). Since corticosterone metabolites are elevated in urine, serum corticosterone levels would be expected to increase in the *Fxr*-null mice fed CA diet, and thus corticosterone levels were determined in serum (Fig. 3E). Indeed, *Fxr*-null mice showed a robust increase in corticosterone level after treatment with the CA diet (changed 24.0 ± 8.3 to 149 ± 76 ng/ml, $P < 0.01$). On the other hand, wild-type mice did not exhibit a significant change in corticosterone levels (changed 13.0 ± 7.0 to 29.0 ± 17.0 ng/ml).

Identification of cholic acid metabolites

Authentic cholic acid metabolites were required for elucidating structure. Tauro-3α,7β,12α-trihydroxycholate (tauro-7-epicholate) and 4 epimers of tauro-3α,6(α/β),7(α/β),12α-tetrahydroxycholate were synthesized as described in "Experimental Procedures." However, two novel metabolites, cholate glucoside ($C_{30}H_{50}O_{10}$, mass error = 3.5 ppm) and taurocholate glucoside ($C_{32}H_{55}NO_{12}S$, mass

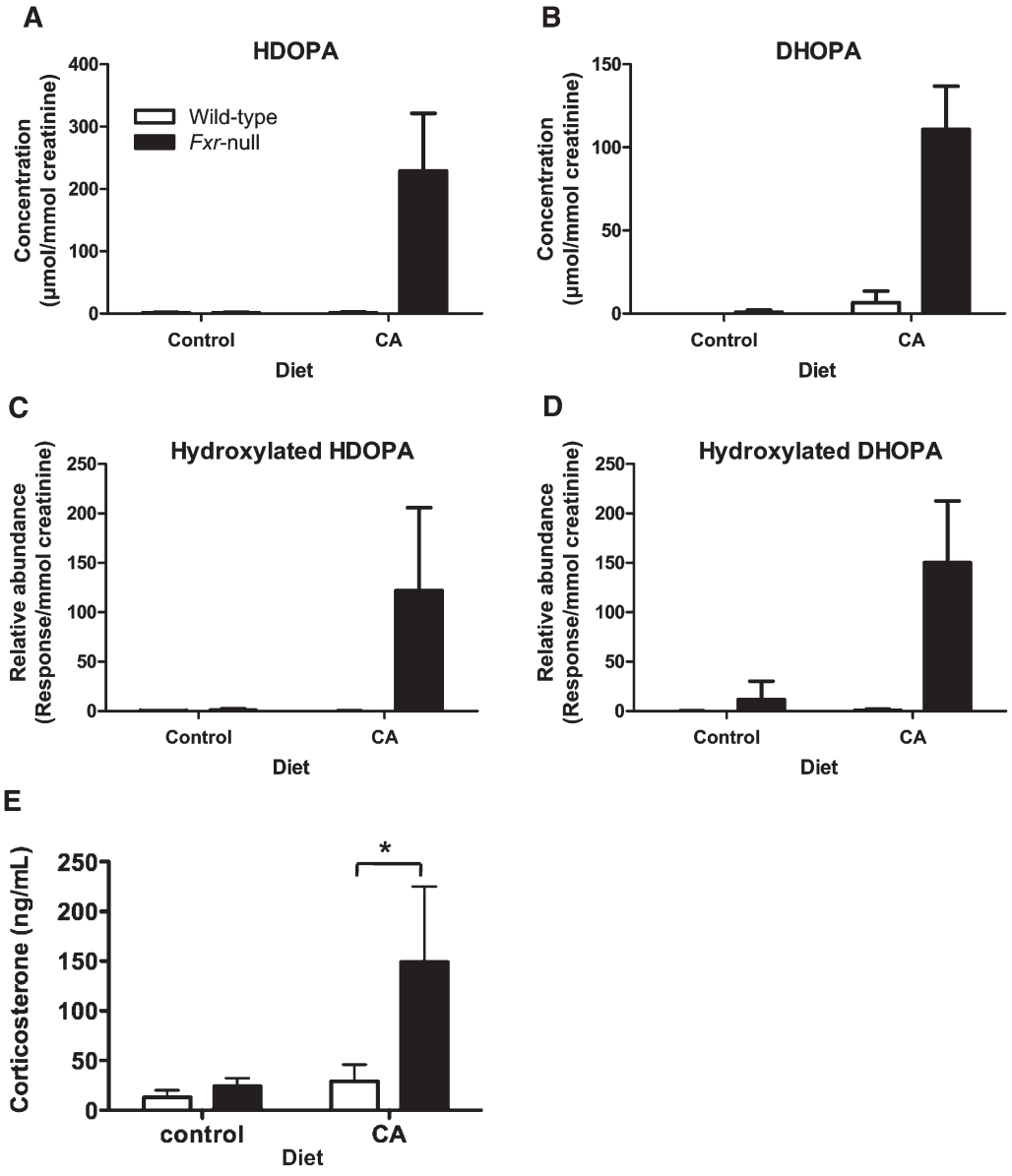

Fig. 3. Quantification of urinary corticosterone metabolites and serum corticosterone in wild-type and *Fxr*-null mice treated with 1% CA or control for 7 days. A: Creatinine-normalized concentration of HDOPA. B: Creatinine-normalized concentration of DHOPA. Concentrations of creatinine, HDOPA, and DHOPA were determined from calibration curve of each metabolite. All concentrations for quantification were normalized to the creatinine concentration (μmol/mmol creatinine). C: Relative abundance of hydroxylated HDOPA was determined by the peak area responses of hydroxylated HDOPA normalized by the creatinine concentration in urine (response/mmol creatinine). D: Relative abundance of hydroxylated DHOPA was determined by the peak area responses of hydroxylated DHOPA normalized by the creatinine concentration in urine (response/mmol creatinine). Data were represented as mean value ± SD (n = 6–12). E: Serum corticosterone levels. The corticosterone levels were measured as described in "Experimental Procedures." Data were expressed as mean value and SD (n = 4–5). Significant difference was determined by one-way ANOVA following Bonferroni's test. $*P < 0.01$ compared with wild-type mice. Open and filled bars represent wild-type and *Fxr*-null mice groups, respectively. CA, cholic acid; DHOPA, 11β,20-dihydroxy-3-oxopregn-4-en-21-oic acid; FXR, farnesoid X receptor; HDOPA, 11β-hydroxy-3,20-dioxopregn-4-en-21-oic acid.

error = 1.9 ppm), could not be synthesized and confirmed by UPLC-MS/MS.

The identities of tauro-3α,7α,12α-trihydroxycholate (taurocholate), tauro-7-epicholate, and tauro-3α,6,7α,12α-tetrahydroxycholate (tauro-3α,6,7α,12α-tetrol) were confirmed by comparison of retention time from authentic compounds and the urinary constituent because cholic acid metabolites are too stable in negative ion mode to generate their tandem mass spectra (**Fig. 4**). Taurocholate and tauro-7-epicholate have identical *m/z* ($[M\text{-}H]^-$ = 514.283) but separable retention time, i.e., 5.39 min (Fig. 4A) and 4.97 min (data not shown), respectively. Among the urinary ions with 514.283 *m/z* ($[M\text{-}H]^-$), Peak **a** had a 4.97 min retention time and was revealed to be identical to

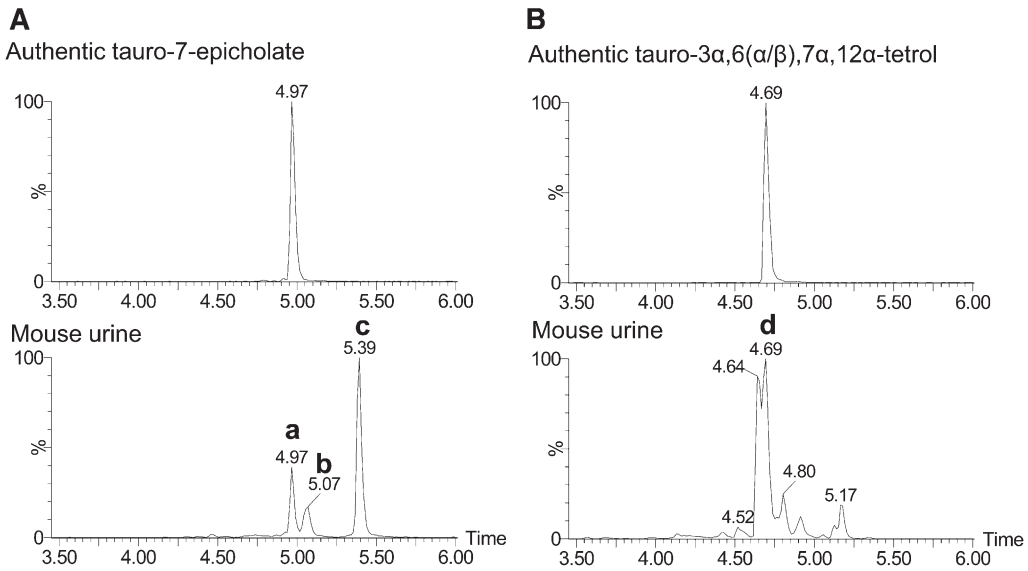

Fig. 4. Identification of tauro-7-epicholate and tauro-3α,6(α/β),7α,12α-tetrol. A: Chromatograms of synthetic tauro-7-epicholate (upper panel) and mouse urine (lower panel). Both ion chromatograms were extracted in the 50 ppm mass range of tauro-7-epicholate (514.2839 *m/z*) in the negative ion mode. B: Chromatograms of synthetic tauro-3α,6(α/β),7α,12α-tetrol (upper panel) and mouse urine (lower panel). Both ion chromatograms were extracted in the 50 ppm mass range of tauro-3α,6(α/β),7α,12α-tetrol (530.2788 *m/z*) in negative ion mode. The values of retention time for several peaks are listed above their respective peak. In mouse urine, several peaks confirmed with authentic compounds are labeled: tauro-7-epicholate (a), tauro-β-muricholate (b), taurocholate (c), and tauro-3α,6(α/β),7α,12α-tetrol (d).

tauro-7-epicholate. Peaks **b** and **c** in Fig. 4A were confirmed with standard compounds of tauro-3α,6α,7β-trihydroxycholate (tauro-β-muricholate) and taurocholate, respectively. Among the four epimers of tauro-3α,6(α/β),7(α/β),12α-tetrol synthesized, both tauro-3α,6α,7α,12α-tetrol and tauro-3α,6β,7α,12α-tetrol had identical retention times (4.69 min) under the chromatographic conditions employed. Peak **d**, the highest among the ions in the extracted chromatogram ($[M-H]^-$ = 530.278) of mouse urine sample, had identical retention time (4.69 min) with the above authentic compounds. Therefore, the identity of taurotetrol that was greatly increased in *Fxr*-null mice after CA feeding was tauro-3α,6(α/β),7α,12α-tetrahydroxycholate (Fig. 4B). The other two epimers, tauro-3α,6α,7β,12α-tetrahydroxycholate and tauro-3α,6β,7β,12α-tetrahydroxycholate did not show the identical retention time to the other peaks extracted with 530.278 *m/z* ($[M-H]^-$).

Quantification of cholic acid metabolites

The concentrations of taurocholate, tauro-7-epicholate, and tauro-3α,6,7α,12α-tetrol as well as creatinine were measured in each urine sample using dehydroxycholate as an internal standard and expressed as μmol/mmol creatinine. Urinary concentrations of taurocholate, tauro-7-epicholate, and tauro-3α,6,7α,12α-tetrol were undetectable in both wild-type and *Fxr*-null mice fed control diet (**Fig. 5**). After feeding the CA diet, taurocholate concentrations were elevated to 46.4 ± 59.5 μmol/mmol creatinine in wild-type mice and to 139 ± 64.4 μmol/mmol creatinine in *Fxr*-null mice, which were statistically significantly different ($P < 0.001$). In contrast to undetectable concentration of tauro-7-epicholate and tauro-3α,6,7α,12α-tetrol in wild-type mice on the CA diet, their concentrations in *Fxr*-null mice on the CA diet was 82.8 ± 68.3 μmol/mmol creatinine for tauro-7-epicholate and 444 ± 322 μmol/mmol creatinine for tauro-3α,6,7α,12α-tetrol (Fig. 5B, C).

Hepatic gene expression

Metabolomic differences in urine between wild-type and *Fxr*-null mice after feeding the CA diet suggested that increased urinary metabolic phenotypes resulted from an adaptive response of *Fxr*-null mice to CA-induced toxicity through alteration of gene expression for metabolic enzymes. Specifically, the highly increased cholic acid metabolite in *Fxr*-null fed CA, tauro-3α,6,7α,12α-tetrol, was a 6-hydroxylated form of taurocholate, which suggested that bile acid-oxidation enzymes such as CYP3A11 and CYP2B10 were induced in *Fxr*-null mice (18). The hepatic expression of *Cyp3a11*, a representative PXR target gene, was elevated significantly by approximately 6-fold in *Fxr*-null mice fed both control and CA diets, compared with wild-type mice fed a control diet (data not shown). The hepatic expression of *Cyp2b10*, a representative constitutive androstane receptor (CAR) target gene, was elevated by approximately 10-fold and 4-fold in *Fxr*-null mice fed control and CA diets, respectively, compared with wild-type mice fed a control diet (data not shown), but these differences were not statistically significant. These expression levels for *Cyp3a11* and *Cyp2b10* were similar to a previous report (18).

Cholestatic hepatotoxicity model

Recent reports revealed that *Fxr*-null mice detoxify accumulating bile acids in the liver by enhanced hydroxyla-

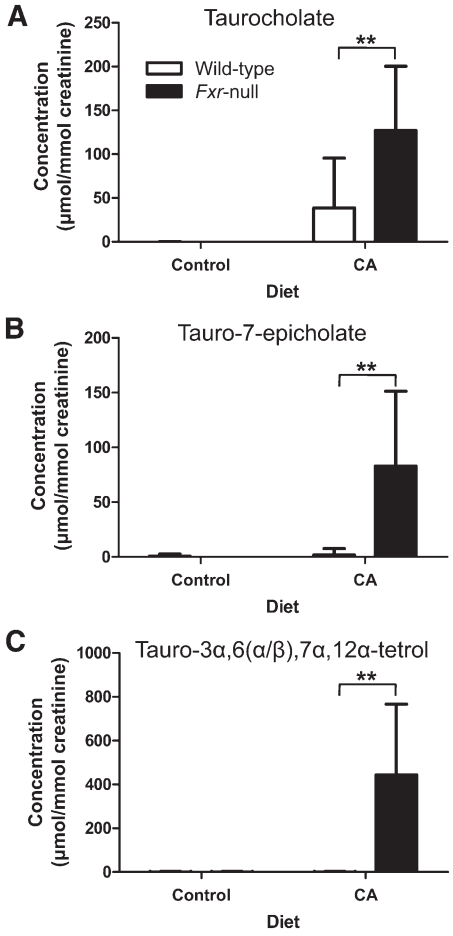

Fig. 5. Quantification of taurocholate, tauro-7-epicholate and tauro-3α,6(α/β),7α,12α-tetrol in urine of wild-type and *Fxr*-null mice treated with 1% CA or control for 7 days. Concentrations of creatinine, taurocholate, and tauro-7-epicholate and tauro-3α,6(α/β),7α,12α-tetrol were determined from calibration curve of each metabolite and normalized to the creatinine concentration (μmol/mmol creatinine). A: Creatinine-normalized concentration of taurocholate. B: Creatinine-normalized concentration of tauro-7-epicholate. C: Creatinine-normalized concentration of tauro-3α,6(α/β),7α,12α-tetrol. Open and filled bars represent wild-type and *Fxr*-null mice groups, respectively. Data were represented as mean value ± SD (n = 6–12). The *P* values were calculated by ANOVA with Bonferroni posttests. $^{**}P < 0.001$ compared with wild-type mice. CA, cholic acid; FXR, farnesoid X receptor.

tion reactions, some of which are catalyzed by CYP3A11, a P450 typically involved in drug metabolism (18). To characterize the effect of enhanced hydroxylation of bile acids on hepatoprotection in *Fxr*-null mice, LCA-induced cholestatic model was used. Because BSEP, regulated by FXR, is highly expressed in wild-type mice but not in *Fxr*-null mice, the CA-induced cholestasis is found only in *Fxr*-null mice. Therefore, administration of LCA, a hydrophobic secondary bile acid, causes intrahepatic cholestasis in wild-type mice as well as in *Fxr*-null mice (19). Male wild-type and *Fxr*-null mice were fed a diet containing 0.6% LCA for 4 days, and their urine was collected for 24 h both prior to and after 3 days on the diet. Blood and liver samples were taken for biochemical assay after 4 days on the diet. The relative abundance of a urinary taurine-conjugated tetrahydroxy bile acid ($[M-H]^-$ = 530.278), which may be derived from LCA, was measured individually in addition to analysis of the relative *Cyp3a11* level and serum ALT activity. A clear correlation (Pearson's correlation coefficient, $r = 0.63$, $P = 0.005$) was observed between individual relative abundance of the taurotetrol and *Cyp3a11* expression levels (**Fig. 6A**). The relative abundance of the taurotetrol was significantly 4.3-fold higher in *Fxr*-null than in wild-type mice ($P = 0.009$). In addition, relative *Cyp3a11* expression levels in liver exhibited a significant increase by 3.8-fold in *Fxr*-null mice on the LCA diet compared with those in wild-type mice on LCA diet ($P < 0.0001$). Moreover, an inverse correlation ($r = -0.85$, $P < 0.0001$) was observed between ALT activity and relative CYP3A11 levels in liver of both wild-type and *Fxr*-null mice (Fig. 6B). Serum ALT activity was 4860 ± 1680 IU/L in wild-type mice and 1960 ± 1090 IU/L in *Fxr*-null mice on LCA diet (40% lower than wild-type mice, $P = 0.0003$). However, serum ALP activity, a typical diagnostic cholestatic marker, was not significantly different between wild-type and *Fxr*-null mice on LCA diet (569 ± 169 and 444 ± 195 IU/L, respectively). Taken together, these data suggested that *Fxr*-null mice eliminate the systemic and hepatic bile acid load more rapidly than wild-type mice by increasing the expression of CYP3A11, resulting in increased hydroxylation of bile acids and less hepatotoxicity than wild-type mice under LCA-induced cholestasis.

DISCUSSION

Global analyses of urinary metabolomes in *Fxr*-null mice compared with their wild-type littermates under conditions of CA loading revealed separation of three groups in a scores plot: control wild-type and *Fxr*-null mice; CA-fed wild-type mice; and CA-fed *Fxr*-null mice. These results suggest that CA feeding markedly changes urinary metabolites in *Fxr*-null mice and, to a lesser degree, in wild-type mice. OPLS analysis between wild-type and *Fxr*-null mice on the CA diet further showed that most of the increased ions were metabolites of *p*-cresol, corticosterone, and CA.

Urinary *p*-cresol comes from dietary polyphenols or tyrosine residues generated by intestinal microorganisms including *Proteus vulgaris*, *Clostridium difficile*, and unidentified species of *Lactobacillus* (20, 21). Urinary *p*-cresol was reported to be one of the dysbiosis markers, including benzoate, hippurate, phenylacetate, and hydroxybenzoate, which are associated with microbial overgrowth (22). More recently, metabolomics analysis revealed *p*-cresol sulfate as being unique to plasma samples of conventional mice compared with samples of germ-free mice (23). In this study, attenuated *p*-cresol conjugates after CA feeding suggested that oral administration of bile acids inhibits the intestinal microbial overgrowth (24). Specifically, CA feeding markedly attenuated urinary *p*-cresol metabolites in wild-type mice but to a lesser extent in *Fxr*-null mice, indicating that CA feeding substantially increases fecal bile acid excretion through induction of bile acid transporters in wild-type mice but to a lesser extent in *Fxr*-null mice, as

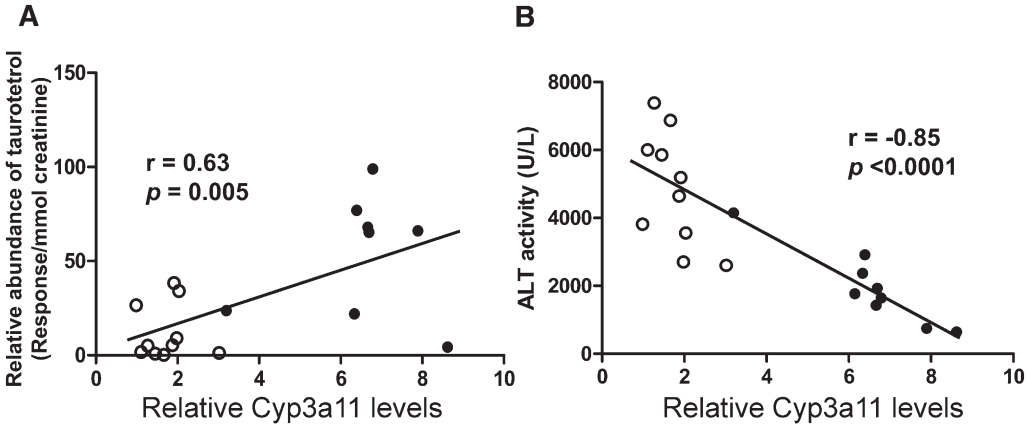

Fig. 6. Correlation plots of hepatic *Cyp3a11* expression with formation of taurotetrol or hepatotoxicity in the cholestatic mouse model induced by LCA. *Fxr*-null and wild-type mice were fed a 0.6% LCA diet or control diet for 4 days and urine and serum samples were collected. A: Correlation between relative CYP3A11 levels and relative abundance of taurotetrol. B: Correlation between relative CYP3A11 levels and ALT activity in serum. Relative CYP3A11 levels were determined by real-time PCR analysis using gene-specific primers and β-actin as the internal control. Relative abundance of taurotetrol was determined by the peak area responses of taurotetrol normalized by the creatinine concentration in urine (response/mmol creatinine). ALT activities were determined as described in "Experimental Procedures." Correlation analysis was constructed in wild-type (open circle) and *Fxr*-null (closed circle) mice fed with LCA. Correlation coefficient, r values and *P* values were calculated by Pearson correlation test. ALT, alanine aminotransferase; FXR, farnesoid X receptor; LCA, lithocholic acid.

revealed in the fecal bile acid excretion rate documented in an earlier study (6).

A dramatic increase of urinary corticosterone metabolites HDOPA and DHOPA, as well as serum corticosterone, was observed only in cholestatic mice (i.e., *Fxr*-null mice fed CA for 7 days). In cholestatic animal models and humans, the hypothalamic-pituitary-adrenal axis was activated by endotoxin and cytokines, such as tumor necrosis factor-α, resulting in an elevation of plasma glucocorticoid concentration (25). Most of the corticosterone present in the blood is excreted into urine and feces as more polar metabolites of corticosterone through an intensive steroid metabolism in liver and gut (26), although there has been only limited information about metabolic pathways of glucocorticoids (27). Therefore, highly increased urinary excretion of HDOPA and DHOPA in acute cholestasis may result from secretion and extensive metabolism of corticosterone. Recently, HDOPA and DHOPA were reported as highly specific biomarkers for activation of PPARα (11). However, high levels of HDOPA and DHOPA in CA-fed *Fxr*-null mice may not be associated with activation of PPARα because the expression of PPARα-target genes such as *Cpt1a* and *Cyp4a10* were not induced by CA feeding (data not shown). Furthermore, a previous study reported that bile acids interfere with transactivation of PPARα at least in part by impairing the recruitment of transcriptional coactivators (28). Hydroxylated metabolites of HDOPA and DHOPA were also highly increased in CA-fed *Fxr*-null mice to an extent similar to that observed with HDOPA and DHOPA. However, an increase of these hydroxylated metabolites were not found in urine from mice treated with the PPARα agonist Wy-14,643 (11). This result indicates that CA-fed *Fxr*-null mice have different metabolic pathways of corticosterone from PPARα-activated mice, possibly mediated by induction of hydroxylation by enzymes such as CYP3A11. However, further investigation should be performed to establish the specific metabolic pathways of corticosterone, HDOPA, and DHOPA in cholestatic mice.

The metabolomics data revealed various CA metabolites as potential markers of cholestasis: taurocholate; tauro-7-epicholate; tauro-3α,6,7α,12α-tetrol; cholate glucoside; and taurocholate glucoside. However, the structures of cholate glucoside and taurocholate glucoside could not be confirmed in this study, thus warranting further investigation. Tauro-7-epicholate and tauro-3α,6,7α,12α-tetrol were identified and quantified as a form of free bile acids in previous reports (18, 29, 30), but their structures in this study were confirmed by comparison with each synthetic conjugated compound. Because bile acids are generally too stable in negative ion mode to generate their tandem mass spectra, identification of structures was performed by comparison of retention time. Although this method is not ideal because of similar structures and similar retention times with each CA metabolite, three compounds with 514.283 *m/z* including taurocholate, tauro-7-epicholate, and tauro-β-muricholate could be distinguished using retention time. In the case of four epimers of tauro-3α,6(α/β),7(α/β),12α-tetrol synthesized in the present study, different retention times were observed between tauro-3α,6α,7β,12α-tetrol and tauro-3α,6β,7β,12α-tetrol, whereas tauro-3α,6α,7α,12α-tetrol and tauro-3α,6β,7α,12α-tetrol had identical retention times under the chromatographic conditions performed here. Nevertheless, tauro-3α,6(α/β),7α,12α-tetrols were observed in urine, plasma, bile or liver tissue of both *Fxr*-null mice and *Bsep*-null mice in previous studies (18, 29). The other taurotetrols, except for tauro-3α,6,7α,12α-tetrol, also existed in a

chromatogram extracted for 530.278 *m/z*, which may be hydroxylated forms of CA in positions other than the 6 position. Marschall et al. had revealed significantly enhanced hydroxylation at the 1β, 2β, 4β, 6α, 6β, 22, or 23 positions of CA in *Fxr*-null mice with biliary obstruction (18). They also exhibited elevated expression of CYP3A11 in *Fxr*-null mice as compared with wild-type mice with biliary obstruction. Human CYP3A4, a homolog to mouse CYP3A11, plays a role of hydroxylation of bile acids at the 6α and 6β positions (31, 32). Therefore, highly expressed CYP3A11 in cholestatic condition was involved in enhanced urinary excretion of hydroxylated bile acids including tauro-3α,6,7α,12α-tetrol.

Several previous reports have clearly demonstrated that induction of CYP3A expression enhances the formation of hydroxylated LCA and protects against severe liver damage induced by LCA (32, 33). In the present study, high expression of CYP3A11 and enhanced urinary excretion of tetrols in *Fxr*-null mice under CA loading suggested that *Fxr*-null mice had an adaptive defense mechanism to detoxify accumulating bile acids in the liver by enhanced hydroxylation probably catalyzed by CYP3A11. However, because wild-type mice under CA loading had increased expression of BSEP and enhanced biliary excretion of bile acids but did not show cholestasis, we could not prove the adaptive hepatoprotective effects against bile acid-induced liver damage in *Fxr*-null mice using the CA loading model. Because LCA feeding induces segmental bile duct obstruction and destructive cholangitis in wild-type mice (34), we observed that serum ALT activity in wild-type mice was significantly higher than that in *Fxr*-null mice using LCA-induced cholestatic mouse model, suggesting that *Fxr*-null mice have a higher capacity to attenuate bile acid-induced hepatotoxicity than do wild-type mice. In addition, the correlation plot of relative abundance of taurotetrol or serum ALT activities with CYP3A11 expression reveals that *Fxr*-null mice are protected against LCA-induced liver damage, possibly mediated by induction of *Cyp3a11* and production of hydroxylated bile acids.

In addition to hydroxylation by CYP3A11, several adaptive mechanisms were activated in cholestatic liver injury and resulted from induction of phase II enzymes and transporters such as SULT2A, OSTα/β, MRP2, MRP3, and MRP4, possibly through activation of PXR, CAR, and VDR (7, 35, 36). Despite various defense responses, the urinary metabolomic data provide an explanation that the enhanced hydroxylation of bile acids by CYP3A11 is one of the major adaptive pathways to detoxify toxic bile acids in cholestatic *Fxr*-null mice. Although the underlying molecular mechanisms of the intrinsic adaptive response to bile acids in *Fxr*-null mice is not fully understood, disruption of FXR, a key regulator for bile acids, increases intrahepatic bile acid concentrations which activate more extensively other nuclear receptors, such as PXR, CAR, and VDR, to enhance the hepatic defense against toxic bile acids (7).

In summary, a metabolomic investigation was conducted on *Fxr*-null mice with CA loading compared with their wild-type counterparts. OPLS analysis of mass spectrometric data matrices revealed that the several metabolites of corticosterone and CA had been highly elevated in *Fxr*-null mice by CA loading but not in wild-type mice. Tauro-3α,6,7α,12α-tetrol, one of the most increased metabolites in *Fxr*-null mice on a CA diet, is a marker for efficient hydroxylation of toxic bile acids possibly by high induction of CYP3A11. Furthermore, LCA-induced toxic models proved that the enhanced expression of *Cyp3a11* is the major defense mechanism to detoxify cholestatic bile acids in *Fxr*-null mice. These results will be useful for identification of biomarkers for cholestasis and for determination of adaptive molecular mechanisms in cholestasis.

REFERENCES

1. Makishima, M., A. Y. Okamoto, J. J. Repa, H. Tu, R. M. Learned, A. Luk, M. V. Hull, K. D. Lustig, D. J. Mangelsdorf, and B. Shan. 1999. Identification of a nuclear receptor for bile acids. *Science.* **284:** 1362–1365.
2. Seol, W., H. S. Choi, and D. D. Moore. 1995. Isolation of proteins that interact specifically with the retinoid X receptor: two novel orphan receptors. *Mol. Endocrinol.* **9:** 72–85.
3. Jelinek, D. F., S. Andersson, C. A. Slaughter, and D. W. Russell. 1990. Cloning and regulation of cholesterol 7 alpha-hydroxylase, the rate-limiting enzyme in bile acid biosynthesis. *J. Biol. Chem.* **265:** 8190–8197.
4. Kullak-Ublick, G. A., B. Stieger, B. Hagenbuch, and P. J. Meier. 2000. Hepatic transport of bile salts. *Semin. Liver Dis.* **20:** 273–292.
5. Wagner, M., P. Fickert, G. Zollner, A. Fuchsbichler, D. Silbert, O. Tsybrovskyy, K. Zatloukal, G. L. Guo, J. D. Schuetz, F. J. Gonzalez, et al. 2003. Role of farnesoid X receptor in determining hepatic ABC transporter expression and liver injury in bile duct-ligated mice. *Gastroenterology.* **125:** 825–838.
6. Sinal, C. J., M. Tohkin, M. Miyata, J. M. Ward, G. Lambert, and F. J. Gonzalez. 2000. Targeted disruption of the nuclear receptor FXR/BAR impairs bile acid and lipid homeostasis. *Cell.* **102:** 731–744.
7. Zollner, G., H. U. Marschall, M. Wagner, and M. Trauner. 2006. Role of nuclear receptors in the adaptive response to bile acids and cholestasis: pathogenetic and therapeutic considerations. *Mol. Pharm.* **3:** 231–251.
8. Zollner, G., M. Wagner, T. Moustafa, P. Fickert, D. Silbert, J. Gumhold, A. Fuchsbichler, E. Halilbasic, H. Denk, H. U. Marschall, et al. 2006. Coordinated induction of bile acid detoxification and alternative elimination in mice: role of FXR-regulated organic solute transporter-alpha/beta in the adaptive response to bile acids. *Am. J. Physiol. Gastrointest. Liver Physiol.* **290:** G923–G932.
9. Idle, J. R., and F. J. Gonzalez. 2007. Metabolomics. *Cell Metab.* **6:** 348–351.
10. Chen, C., F. J. Gonzalez, and J. R. Idle. 2007. LC-MS-based metabolomics in drug metabolism. *Drug Metab. Rev.* **39:** 581–597.
11. Zhen, Y., K. W. Krausz, C. Chen, J. R. Idle, and F. J. Gonzalez. 2007. Metabolomic and genetic analysis of biomarkers for peroxisome proliferator-activated receptor alpha expression and activation. *Mol. Endocrinol.* **21:** 2136–2151.
12. Cho, J. Y., D. W. Kang, X. Ma, S. H. Ahn, K. W. Krausz, H. Luecke, J. R. Idle, and F. J. Gonzalez. 2009. Metabolomics reveals a novel vitamin E metabolite and attenuated vitamin E metabolism upon PXR activation. *J. Lipid Res.* **50:** 924–937.
13. Needs, P. W., and G. Williamson. 2001. Syntheses of daidzein-7-yl beta-D-glucopyranosiduronic acid and daidzein-4′,7-yl di-beta-D-glucopyranosiduronic acid. *Carbohydr. Res.* **330:** 511–515.
14. Iida, T., I. Komatsubara, S. Yoda, J. Goto, T. Nambara, and F. C. Chang. 1990. Potential bile acid metabolites. 16. Synthesis of stereoisomeric 3 alpha,6,7,12 alpha-tetrahydroxy-5 beta-cholanoic acids. *Steroids.* **55:** 530–539.
15. Xue, C. B., and W. F. Degrado. 1995. An efficient synthesis of glycoprotein IIb/IIIa inhibitor DMP728. A novel synthesis of N^{α}-methylarginine-containing peptide. *J. Org. Chem.* **60:** 946–952.
16. Dayal, B., K. R. Rapole, G. Salen, S. Shefer, G. S. Tint, and S. R. Wilson. 1995. Microwave-induced rapid synthesis of bile-acid conjugates. *Synlett.* 861–862.
17. Guo, G. L., G. Lambert, M. Negishi, J. M. Ward, H. B. Brewer, Jr., S. A. Kliewer, F. J. Gonzalez, and C. J. Sinal. 2003. Complementary roles of farnesoid X receptor, pregnane X receptor, and consti-

tutive androstane receptor in protection against bile acid toxicity. *J. Biol. Chem.* **278:** 45062–45071.
18. Marschall, H. U., M. Wagner, K. Bodin, G. Zollner, P. Fickert, J. Gumhold, D. Silbert, A. Fuchsbichler, J. Sjovall, and M. Trauner. 2006. Fxr(−/−) mice adapt to biliary obstruction by enhanced phase I detoxification and renal elimination of bile acids. *J. Lipid Res.* **47:** 582–592.
19. Hofmann, A. F. 2004. Detoxification of lithocholic acid, a toxic bile acid: relevance to drug hepatotoxicity. *Drug Metab. Rev.* **36:** 703–722.
20. Martin, A. K., J. A. Milne, and P. Moberly. 1983. The origin of urinary aromatic compounds excreted by ruminants. 4. The potential use of urine aromatic acid and phenol outputs as a measure of voluntary food intake. *Br. J. Nutr.* **49:** 87–99.
21. Ward, L. A., K. A. Johnson, I. M. Robinson, and M. T. Yokoyama. 1987. Isolation from swine feces of a bacterium which decarboxylates p-hydroxyphenylacetic acid to 4-methylphenol (p-cresol). *Appl. Environ. Microbiol.* **53:** 189–192.
22. Lord, R. S., and J. A. Bralley. 2008. Clinical applications of urinary organic acids. Part 2. Dysbiosis markers. *Altern. Med. Rev.* **13:** 292–306.
23. Wikoff, W. R., A. T. Anfora, J. Liu, P. G. Schultz, S. A. Lesley, E. C. Peters, and G. Siuzdak. 2009. Metabolomics analysis reveals large effects of gut microflora on mammalian blood metabolites. *Proc. Natl. Acad. Sci. USA.* **106:** 3698–3703.
24. Lorenzo-Zuniga, V., R. Bartoli, R. Planas, A. F. Hofmann, B. Vinado, L. R. Hagey, J. M. Hernandez, J. Mane, M. A. Alvarez, V. Ausina, et al. 2003. Oral bile acids reduce bacterial overgrowth, bacterial translocation, and endotoxemia in cirrhotic rats. *Hepatology.* **37:** 551–557.
25. Swain, M. G., and M. Maric. 1996. Tumor necrosis factor-alpha stimulates adrenal glucocorticoid secretion in cholestatic rats. *Am. J. Physiol.* **270:** G987–G991.
26. Touma, C., N. Sachser, E. Mostl, and R. Palme. 2003. Effects of sex and time of day on metabolism and excretion of corticosterone in urine and feces of mice. *Gen. Comp. Endocrinol.* **130:** 267–278.
27. Han, A., A. Marandici, and C. Monder. 1983. Metabolism of corticosterone in the mouse. Identification of 11 beta, 20 alpha-dihydroxy-3-oxo-4-pregnen-21-oic acid as a major metabolite. *J. Biol. Chem.* **258:** 13703–13707.
28. Sinal, C. J., M. Yoon, and F. J. Gonzalez. 2001. Antagonism of the actions of peroxisome proliferator-activated receptor-alpha by bile acids. *J. Biol. Chem.* **276:** 47154–47162.
29. Perwaiz, S., D. Forrest, D. Mignault, B. Tuchweber, M. J. Phillip, R. Wang, V. Ling, and I. M. Yousef. 2003. Appearance of atypical 3 alpha,6 beta,7 beta,12 alpha-tetrahydroxy-5 beta-cholan-24-oic acid in spgp knockout mice. *J. Lipid Res.* **44:** 494–502.
30. Ridlon, J. M., D. J. Kang, and P. B. Hylemon. 2006. Bile salt biotransformations by human intestinal bacteria. *J. Lipid Res.* **47:** 241–259.
31. Bodin, K., U. Lindbom, and U. Diczfalusy. 2005. Novel pathways of bile acid metabolism involving CYP3A4. *Biochim. Biophys. Acta.* **1687:** 84–93.
32. Xie, W., A. Radominska-Pandya, Y. Shi, C. M. Simon, M. C. Nelson, E. S. Ong, D. J. Waxman, and R. M. Evans. 2001. An essential role for nuclear receptors SXR/PXR in detoxification of cholestatic bile acids. *Proc. Natl. Acad. Sci. USA.* **98:** 3375–3380.
33. Staudinger, J. L., B. Goodwin, S. A. Jones, D. Hawkins-Brown, K. I. MacKenzie, A. LaTour, Y. Liu, C. D. Klaassen, K. K. Brown, J. Reinhard, et al. 2001. The nuclear receptor PXR is a lithocholic acid sensor that protects against liver toxicity. *Proc. Natl. Acad. Sci. USA.* **98:** 3369–3374.
34. Fickert, P., A. Fuchsbichler, H. U. Marschall, M. Wagner, G. Zollner, R. Krause, K. Zatloukal, H. Jaeschke, H. Denk, and M. Trauner. 2006. Lithocholic acid feeding induces segmental bile duct obstruction and destructive cholangitis in mice. *Am. J. Pathol.* **168:** 410–422.
35. Kitada, H., M. Miyata, T. Nakamura, A. Tozawa, W. Honma, M. Shimada, K. Nagata, C. J. Sinal, G. L. Guo, F. J. Gonzalez, et al. 2003. Protective role of hydroxysteroid sulfotransferase in lithocholic acid-induced liver toxicity. *J. Biol. Chem.* **278:** 17838–17844.
36. Makishima, M., T. T. Lu, W. Xie, G. K. Whitfield, H. Domoto, R. M. Evans, M. R. Haussler, and D. J. Mangelsdorf. 2002. Vitamin D receptor as an intestinal bile acid sensor. *Science.* **296:** 1313–1316.